Bulgarian Chemical Communications, Volume 51, Special Issue F (pp. 55 - 62) 2019

Simulations of the macroscopic energy migration diffusion characteristics in upconversion core-shell nanostructures

J. F. Liu, T. R. Fu*

Tsinghua University, Department of Energy and Power Engineering, Key Laboratory for Thermal Science and Power Engineering of Ministry of Education, Beijing, China

Lanthanide-doped upconversion nanostructures have attracted much attention due to their excellent upconversion capabilities to convert low energy photons to high energy photons for a wide variety of optical applications. Although classical macroscopic rate equations have been used to describe the dominant upconversion energy transfer mechanism between the sensitizers and activators by assuming infinitely fast energy migration, these models still do not accurately characterize the upconversion dynamics of core-shell nanostructures. Therefore, this paper models the upconversion luminescence in core-shell nanostructures using improved macroscopic rate equations that simultaneously consider the energy migration and energy transfer. The macroscopic model provides an effective way to design the upconversion luminescence characteristics of core-shell nanostructures from fundamental insights that is more convenient than other simulation or microscopic models. The model was used to study $NaYF_4$: Yb^{3+}, Er^{3+} core-shell nanostructures. The energy migration characteristics among the sensitizers in the core-shell nanostructure were analyzed to understand the upconversion emission decay lifetimes, emission intensities and time-resolved spatial gradients of the excited ion population density that depend on the structure, shell thickness and excitation power. The analysis provides further understanding of the energy migration mechanism for improving the upconversion luminescence of core-shell nanostructures.

Keywords: Upconversion, energy transfer, energy migration, Grant's macroscopic rate equations, diffusion

INTRODUCTION

Lanthanide-doped upconversion (UC) materials that convert low energy photons into high energy photons have attracted much attention due to their high photon stability, large anti-Stokes shifts, long lifetimes and sharp band emissions [1, 2]. They are very promising materials for a wide variety of optical applications such as 3D displays [3], super-resolution imaging [4], biomarkers and drug carriers [5, 6], anti-counterfeiting [7] and solar cells [8]. Core multi-shell upconversion nanostructures are in demand for controlling nano-scale interactions among Ln^{3+} ions to manipulate their UC characteristics including their spectra, intensities, lifetimes and efficiencies [9, 10]. Many composite nanosystems have been developed using UC nanostructures and other nanomaterials including quantum dots [11], nano-phosphors [10, 12], and metal nanostructures [13] that offer new opportunities to manipulate the energy emissions and boost the quantum efficiency.

In upconversion systems having sensitizers (S ions) and activators (A ions), the S-A energy transfers (ET) have long been recognized as the major factor producing the upconverted photons, while the energy migration (EM) among the sensitizers has always been modelled as infinitely fast which neglected Grant's macroscopic rate equations [14]. Although upconversion systems are known to have migration-assisted energy transfer, previous studies have been unable to directly prove its effect on the UC dynamics in the bulk material. The significant effect of energy migration is beginning to become evident in nanostructures. The energy migration design in the nanostructures may provide an effective way to manipulate the UC dynamic characteristics. Wang *et al.* [15] constructed an orthorhombic KYb_2F_7:Er^{3+} nanostructure with Ln^{3+} distributed in tetrad clusters which confined the excitation migration among the Yb^{3+} and minimized the concentration quenching. Chen *et al.* [16] proposed a $NaYF_4$@ $NaYF_4$:Tm^{3+}@ $NaYF_4$ nanostructure in which the excitation migration was confined to the middle layer which produced intense ultraviolet UC emissions. Zuo *et al.* [17, 18] and Zhou *et al.* [19] designed a series of multi-layer nanostructures to illustrate the dependence of the UC luminescence on the shell layer parameters to provide direct evidence of the influence of the energy migration and to demonstrate its usefulness in tuning the emission dynamics in nanostructures. However, the traditional Grant's macroscopic dynamic model and microscopic theoretical models (for example, the Inokuti-Hirayama model, the Zusman model, and the Yokota model) are unable to describe the UC luminescence processes related to the energy migration in core-shell nanostructures. This

* To whom all correspondence should be sent:
trfu@mail.tsinghua.edu.cn

difficulty in developing analytical expressions for UC luminescence processes has been overcome by using Monte-Carlo simulations to describe the macroscopic UC luminescence processes by statistically analysing the microscopic interactions among multiple ions in the core-shell nanostructures. However, the Monte-Carlo simulations depend on accurate microscopic parameters to describe the complex coupling of the energy transitions and transfers among the ions. The spatial energy transfer and migration macroscopic model [20] was recently proposed to describe the UC luminescence dynamics in core-shell nanostructures with the predictions verified experimentally. The present study investigated the UC luminescence characterization in core-shell nanostructures using this macroscopic rate equation model to simultaneously consider the energy migration and energy transfer in $NaYF_4$: Yb^{3+}/Er^{3+} core-shell nanostructures. The model predicts the upconversion emission decay lifetimes, emission intensities, and time-resolved spatial gradients of the excited ion population density as functions of the structure, shell thickness and excitation powers considering the energy migration between sensitizers. The analysis is useful for understanding the energy migration mechanism and manipulating the upconversion luminescence characteristics of core-shell nanostructures from fundamental principles.

THEORETICAL MODELS

In upconversion systems consisting of sensitizers and activators, the ET progress is recognized as the major factor producing upconverted photons, while EM processes are also essential for the system to maintain the UC luminescence. In core-shell UC nanostructures with non-uniform distributions of doped Ln^{3+}, the EM process is not fast enough which results in non-uniform distributions of the excited sensitizers during the ET process. The long-range EM occurs across units in the core-shell nanostructure with a net excitation energy flux between adjacent units. The spatial energy transfer and migration macroscopic model [20] treats the net excitation energy migration among units as gradient-driven diffusion arising from the population density spatial gradient of the excited sensitizers. A spatial migration diffusion term is introduced into the model to predict the change rates of the excited ion population densities in the different spatial regions (core, shell and shell boundary) for the core-shell nanostructure as [20]:

$$\begin{cases} \dot{N}_{S2}(r,t) = q\sigma N_{S1} - W_{S2}N_{S2} + k_{SS}\nabla^2 N_{S2} \\ -\sum_{y\in(1\ldots m)} W_{S2-Ay}N_{S2}N_{Ay} + \sum_{y\in(1\ldots m)} W_{Ay-S1}N_{Ay}N_{S1}; \ \text{core} \\ \dot{N}_{S2}(r,t) = q\sigma N_{S1} - W_{S2}N_{S2} + k_{SS}\nabla^2 N_{S2}; \qquad \text{shell} \\ \dot{N}_{S2}(r,t) = q\sigma N_{S1} - W_{S2-b}N_{S2} + k_{SS}\nabla^2 N_{S2}; \qquad \text{shell surface} \\ \dot{N}_{Ay}(r,t) = -W_{Ay}N_{Ay} + \psi_y, \ 2 \le y \le m; \qquad \text{core} \\ \sum_{x\in(1,2)} \dot{N}_{Sx}(r,t) = 0, \ \sum_{y\in(1\ldots m)} \dot{N}_{Ay}(r,t) = 0 \end{cases} \quad (1)$$

where $W_{S2\text{-}b}$ is the sensitizer surface relaxation rate arising from the surface-related interactions between S ions and surface defects, organic ligands and solvents, k_{SS} is defined as the diffusion constant of S ions representing the long-range effects of excitation migration. Due to the combination of the long-range macroscopic excitation migration diffusion term ($k_{SS}\nabla^2 N_{S2}$) and the macroscopic energy transfer terms (containing rates of $W_{S2\text{-}Ay}$ and $W_{Ay\text{-}S1}$), the model can be used to describe the spatial and temporal UC luminescence characteristics of core-shell nanostructures. This model more accurately describes the UC characteristics in nanostructures than the traditional Grant's macroscopic rate equations or Monte-Carlo simulations.

SIMULATIONS AND DISCUSSION

The core multi-shell nanostructures may be modified to manipulate the UC characteristics. However, most research has focused on the experimental studies of UC nanostructure designs, which has greatly increased the research times and provided limited information. Simulations can provide more information in shorter times to predict the UC characteristics of nanostructures. In this work, the macroscopic diffusion model was realized by a MATLAB program employing a time-marching method and a finite volume difference scheme to simulate the UC luminescence emission dynamics of core multi-shell nanoparticles for various core-shell structures, sizes and excitation conditions. The simulations considered three upconversion nanoparticles with $NaYF_4$: Yb^{3+}, Er^{3+} (Yb^{3+} as sensitizer and Er^{3+} as activator) using the designs shown in Fig.1: NP-I, $NaYF_4$: 20% Yb^{3+}, 2% Er^{3+}@$NaYF_4$ core/inert shell; NP-II, $NaYF_4$: 20% Yb^{3+}, 2% Er^{3+}@ $NaYF_4$: 20% Yb^{3+} core/active shell and NP-III, $NaYF_4$: 20% Yb^{3+}, 2% Er^{3+}@$NaYF_4$: 20% Yb^{3+}@ $NaYF_4$ core/active shell/inert shell. The predictions were then compared with measurements of the emission characteristics.

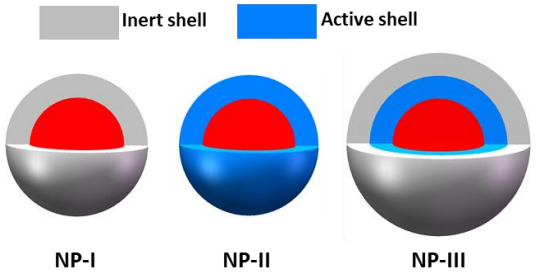

Fig.1. Sketches of the NP-I, NP-II and NP-III nanostructures

Model verification

The parameters in Eq.(1), including the relaxation rates and the macroscopic energy transfer rates, were determined previously [20] and used here to simulate the UC emission spectra curves of all three nanostructure samples with 980 nm pulsed/continuous excitation. This section further verifies the accuracy of the rate equation model in Eq.(1) against experimental data using the known parameters to predict the steady-state upconversion emission characteristics which clarify the detailed interactions among the various levels.

The core diameters of the NP-I and NP-II samples were all 60 nm in the experiments. The inert shell thickness in NP-I was greater than 10 nm and the active shell thickness in NP-II was 6.6 nm. The luminescence properties of the samples were studied in the colloidal state. The steady-state spectra were measured using the Andor Shamrock SR-500i imaging spectrometer. A 980 nm CW laser was focused onto the UC samples as the excitation light to measure the steady-state upconversion emission spectra at various excitation powers. The red/654 nm ($^4F_{9/2}\rightarrow{}^4I_{15/2}$) and green/540 nm ($^2H_{11/2}$, $^4S^{3/2}\rightarrow{}^4I_{15/2}$) upconversion emissions dominated in the experiments so the 654 nm and 540 nm UC emissions are the focus of the analyses. Fig.2a compares the measured and simulated data for the intensity ratios of the 654 nm emissions to the 540 nm emissions obtained using the the rate equation model in Eq. (1) at various steady excitation power densities of 1.8~17.8 W/cm^2. The simulated emission ratios agree reasonably with the experimental data.

For multi-step energy transfer processes, the luminescence emission intensity, I, is usually proportional to the n^{th} power of the excitation power, P, that is $I \propto P^n$. For the 540 nm green emissions of NP-I, the power index of the *I-P* curve from the simulations was 1.15 which is close to the measured value of 1.12 when the NP-I sample was excited at weak power densities below 10 W/cm^2, as shown in Fig.2b. The predicted index, n, then decreased as the excitation power density increased in the power range of (10~10^4 W/cm^2). These trends are consistent with other reported experimental data. The agreement between the theoretical and experimental results for the steady luminescence emissions for the NP-I sample verifies the rate equation model applicability.

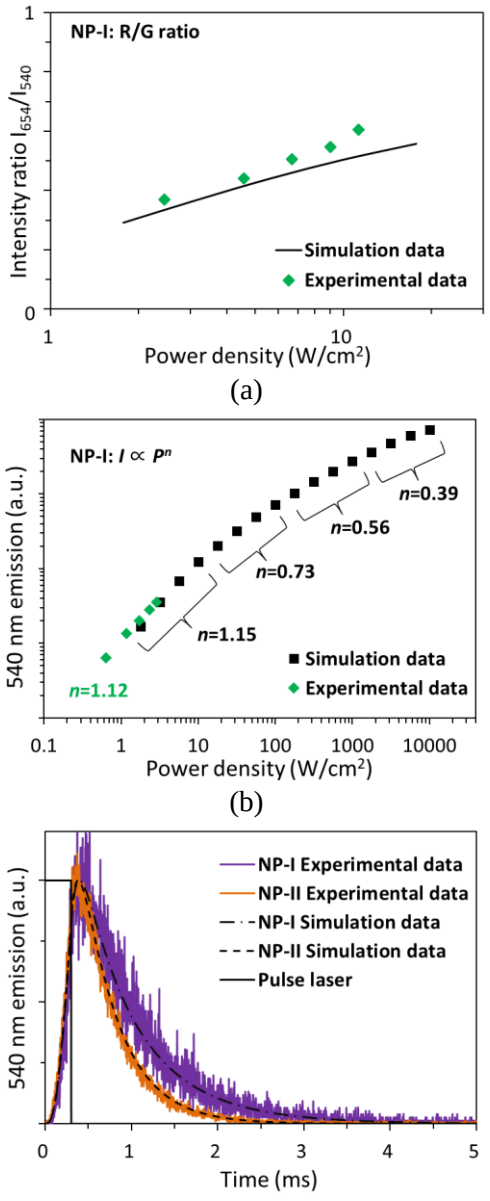

Fig.2. (a) Red/Green emission intensity ratios for NP-I; (b) I-P relations for NP-I for 540 nm green emissions; (c) 540 nm UC emission decay curves for NP-I and NP-II with 980 nm pulsed excitation

The luminescence decay characteristics shown by the simulated 540 nm green emission decay curves for the NP-I and NP-II samples also agree well with the experimental results for 980 nm pulsed excitation (laser power, 11.1 W/cm^2; pulse cycle, 10 ms; pulse width, 300 μs) as shown in

Fig.2c. The simulation results based on Eq. (1) show that the active shell of the NP-II sample shortens the 540 nm emission decay time compared with that of the NP-I sample with the inert shell. The experimental observations of the energy migration and surface quenching effects in the core-shell nanostructures were numerically verified based on Eq. (1). Therefore, the verified model can be used to predict the emission characteristics of the nanostructure structures.

Influence of the multi-shell structure on the emission dynamics

The active shell with Yb^{3+} doping (for example, the NP-II and NP-III nanostructures) can be used to modulate the emissions and tune the lifetime by incorporating two additional pathways for the energy migration across the core-shell interface with surface-related quenching at the shell boundary. The model was used to investigate how these two mechanisms affect the upconversion dynamics with quantitative characterizations of the UC mechanisms in Ln^{3+} doped UC nanoparticles (UCNPs).

In the simulations, the NP-II UCNPs were assumed to be spherical with the same core diameter of 20 nm and different active shell thicknesses (5 nm, 10 nm and 15 nm). The 3-layer nanostructure of the NP-III UCNPs was assumed to have a thick epitaxial inert $NaYF_4$ shell that prevented surface-related quenching of Yb^{3+} to examine the effect of the energy migration in the structure on the upconversion luminescence. The excitation conditions were (1) CW 980 nm laser power density of 100 W/cm^2 for steady-state upconversion emissions and (2) Pulsed 980 nm laser power density peaks of 100 W/cm^2~5×10^4 W/cm^2 with a pulse duration of 1 μs for transient upconversion emission decay curves.

Yb^{3+} and Er^{3+} codoped systems have bright red and green upconversion luminescence. Fig.3 shows the simulated green/540 nm and red/654 nm UC emission decay curves of NP-II with various active shell thicknesses of (5 nm~15 nm) and the same excitation power of 5×10^4 W/cm^2. The abscissa represents the process time. The rising edges of the UC emissions are delayed and the emission decay lifetimes grow longer with increasing active shell thickness. The decay lifetimes of the 540 nm emissions increase from 425 μs to 635 μs while the lifetimes of the 654 nm emissions increase from 523 μs to 688 μs when the shell thickness increases from 5 nm to 15 nm. These trends agree with the experimental observations of Zuo et al. [17]. Although the surface quenching effect with thicker shells with a larger surface area may accelerate the emission decay, a thicker active shell absorbs more excitation power which strengthens the UC emissions. On the other hand, the excitation energy in a thicker shell takes longer to migrate to the core across the core-shell interface. Therefore, the energy migration diffusion mechanisms of Yb^{3+} account for the prolonged luminescence characteristics. The energy migration diffusion strongly depends on the excited Yb^{3+} population density distribution while the boundary condition determines the diffusion direction. Therefore, different excited Yb^{3+} population density distributions will lead to energy migration diffusion forward towards the core due to the UC emissions or backwards towards the surface of the active shell due to surface quenching. These combined effects increase the UC luminescence of Er^{3+} and prolong the emission decay lifetimes in active shells doped with Yb^{3+}.

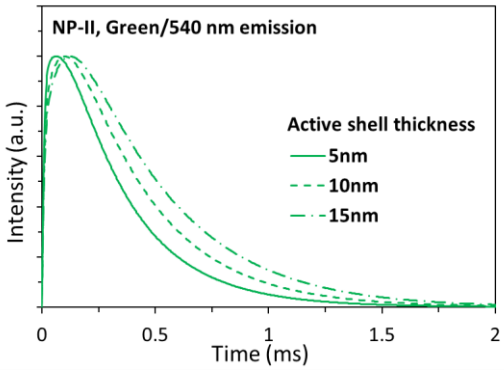

(a)

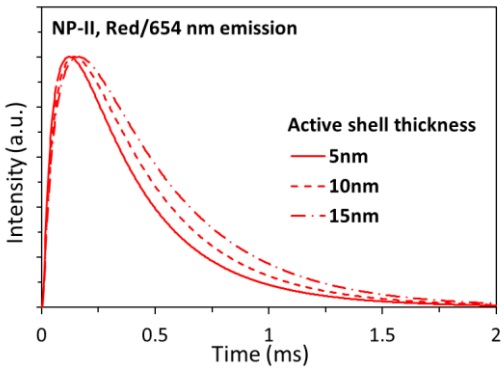

(b)

Fig.3. Simulated (a) 540 nm and (b) 654 nm UC emission decay curves for NP-II with an excitation power of 5×10^4 W/cm^2

Fig.4 shows the simulated green/540 nm UC emission decay curves of NP-II with the same active shell thickness (5 nm) and various pulse

excitation powers (100 W/cm^2 ~5×10^4 W/cm^2). The rising edge of the UC emissions occurs earlier while the emission decay lifetime is approximately constant with increasing excitation power. Thus, the excitation power has little effect on the emission decay rate. The rising edge time changes as the Yb^{3+} in the system becomes more active with high energy excitation rates. Initially, Yb^{3+} in the spherical core reaches its peak earlier by faster energy migration from the shell to the core. Thus, the energy migration has a greater effect on the rising edge time than the surface-related quenching.

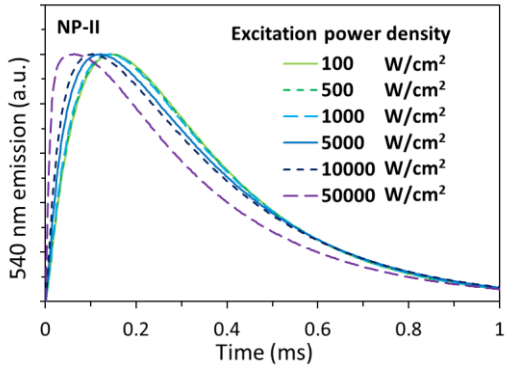

Fig.4. Simulated 540 nm UC emission decay curves of NP-II with an active shell thickness of 5 nm

The influence of the multi-layer shell on the nanostructure emission dynamics is further illustrated by the results in Fig.5 which show the simulated green/540 nm UC emission curves and the NIR/1μm DC (downconversion) emission decay curves for nanostructures NP-II (a single active shell) and NP-III (active-inert two layer shell) with various active shell thicknesses of (5 nm~15 nm) and the same excitation power density of 5×10^4 W/cm^2. The results illustrate that the surface-related quenching of Yb^{3+} is effectively prevented by the additional inert shell in nanoparticle NP-III which lengthens the lifetimes of the UC and DC emissions for nanoparticle NP-III compared to those for nanoparticle NP-II. Actually surface deactivation caused by surface defects, organic ligands and solvents will provide additional relaxation pathways for the excited Yb^{3+}, which directly shortens the Yb^{3+} lifetimes and indirectly reduces the total excitation energy migrated to Er^{3+}. When protected by the inert shell, the increasing active shell thickness of nanoparticle NP-III still leads to longer emission decay lifetimes. Therefore, increasing the active shell thickness with or without the inert shell, the energy migration of the Yb^{3+} always prolongs the luminescence.

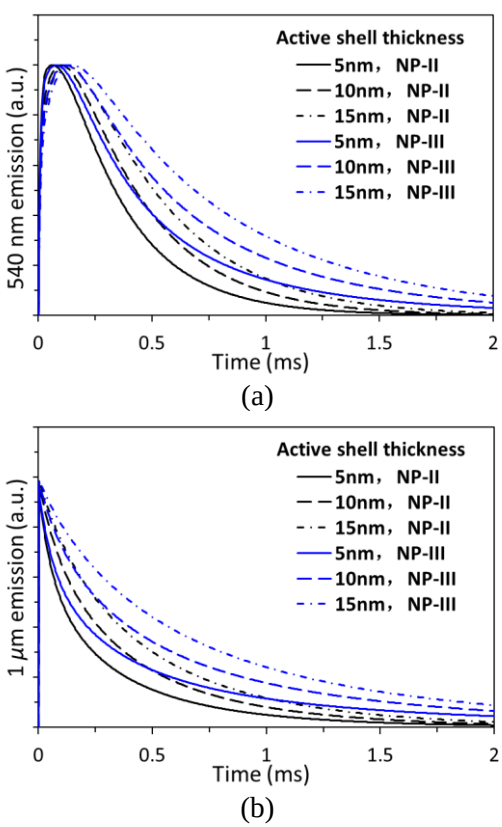

Fig.5. Simulated 540 nm UC emission curves (a) and NIR/1 μm DC emission (b) decay curves of nanostructures NP-II and NP-III

The effect of the core-shell structure design on the luminescence intensity is demonstrated in Fig.6 which shows the simulated green/540 nm steady-state UC emission intensities represented by the population densities of the corresponding energy level N_{A6} for all three nanostructures (NP-I, NP-II, and NP-III) and various active shell thicknesses (5 nm~15 nm) with CW 980 nm laser excitation of 100 W/cm^2. The simulations show that the active shell enhances the luminescence intensity 1.48 fold for NP-II with the 5 nm active shell thickness compared to the NP-I design with the same shell thickness and that the third inert shell layer wrapped around the active shell reduces the surface relaxation of Yb^{3+} which increases the luminescence 1.87 fold for NP-III with the 5 nm active shell thickness compared to the NP-I design with the same shell thickness. Therefore, the emission intensity of NP-III is largest while that of NP-I is smallest. In addition, the luminescence emission intensity increases with the active shell thickness for both the two-layer (NP-II) and three-layer (NP-III) nanostructures. The luminescence increases is 1.82 fold for NP-II and 1.89 fold for NP-III when the active shell thickness is increased from 5 nm to 15 nm.

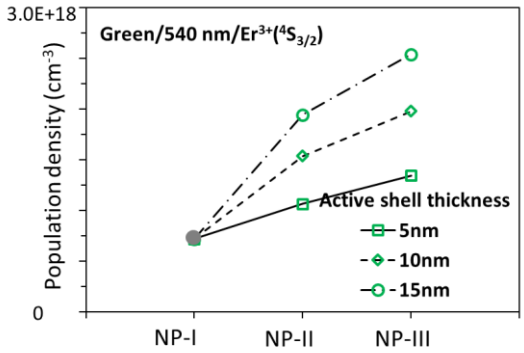

Fig.6. Simulated 540 nm steady-state UC emission intensities for all three nanostructures with 100 W/cm^2 power density

Energy migration in core multi-shell UC nanostructures

In the core-shell nanostructures, the energy migration is related to the excited Yb^{3+} population density distribution. From Eq.(1), the time-resolved spatial gradient of the excited Yb^{3+} population density, dN_{Yb}/dr at the core-shell interface reflects the energy migration diffusion direction at the interface for whether the excitation energy migrates forwards from the shell to the core or backwards from the core to the shell. Fig.7 shows the simulated spatial gradients of the excited Yb^{3+} population density at the core-shell interface for the NP-II and NP-III nanostructures during the emission decay process for various active shell thicknesses.

The gradient dN_{Yb}/dr decreases with time during the emission decay process (0~1.0 ms) and increases with the active shell thickness for both nanostructures. The energy diffusion goes in the same direction during the entire luminescence decay process for NP-III with the active shell and the inert shell, but reverses direction in NP-II with just a single active shell. The direction reverses since the excited Yb^{3+} in the NP-II core relax by transferring excitation energy to the adjacent Er^{3+} while the excited Yb^{3+} in the shell relax by transferring excitation energy to the surface quenchers. When the latter process is faster, the population density distribution of the excited Yb^{3+} reverses after some time. For NP-III, the lack of Yb^{3+} surface quenching leads to the excited Yb^{3+} population density always being higher in the active shell; thus, the energy migration direction remains unchanged. For NP-II, the direction reverses at t_0 equal to 275 μs for the 5 nm active shell thickness, 625 μs for the 10 nm thickness and 890 μs for the 15 nm thickness. Thus, the reversal time increases with the active shell thickness which shows that more excitation energy is converted to the upconversion luminescence in thicker shell structures.

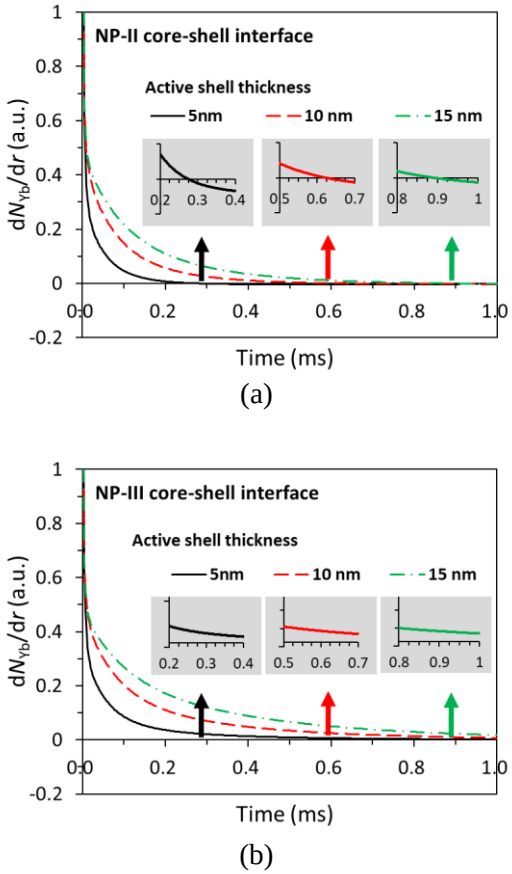

Fig.7. Spatial gradients of the excited Yb^{3+} population density at the core-shell interface, (a) NP-II and (b) NP-III

CONCLUSIONS

The current investigation modelled core-shell nanostructures made of $NaYF_4$ doped with Yb^{3+} and Er^{3+}. The model predicted the upconversion emission decay lifetimes, intensity profiles and time-resolved spatial gradients of the excited Yb^{3+} population density for various structures, shell thicknesses and excitation powers.

The trends of the simulated emission decay curves agree well with measured data. The simulations show that the combined effects of the energy migration diffusion and the surface-related quenching promote the UC luminescence of Er^{3+} in active shells doped with Yb^{3+} and lengthen the emission decay lifetimes. The surface-related quenching of Yb^{3+} is effectively prevented by the additional inert shell in nanoparticle NP-III which leads to longer lifetimes of the UC and DC emissions than for nanoparticle NP-II. With and

without the inert shell, the energy migration diffusion mechanisms of Yb^{3+} in thicker active shells prolong the luminescence and enhance the emission intensity. The simulations also illustrate that the active shell enhances the luminescence intensity and that the inert shell wrapped around the active shell reduces the surface relaxation of Yb^{3+} which increases the luminescence. The predicted time-resolved spatial gradients of the excited Yb^{3+} population density distributions show when the energy excitation migrates forwards from the shell to the core or backwards from the core to the shell due to reversal of the excitation migration direction in the nanoparticles with the active shell. This improved macroscopic model provides an effective method for designing the upconversion luminescence characteristics of core-shell nanostructures from the fundamental physics that is more convenient and accurate than other simulation models or microscopic models.

ACKNOWLEDGEMENTS

The work was supported by the National Natural Science Foundation of China (No. 51976097) and the Science Fund for Creative Research (No. 51621062). The authors have no competing interests to declare.

NOMENCLATURE

N_{Sx}	sensitizer population density in the ground energy level ($x=1$) or in the excited energy level ($x=2$)
N_{Ay}	activator population density in the ground energy level ($y=1$) or in other excited energy levels ($y=2...m$)
q	excitation power density
σ	absorption cross section
r	space coordinates
t	time coordinates
W_{S2}	total relaxation rate of excited sensitizers
W_{Ay}	total relaxation rates of excited activators
$W_{S2\text{-}Ay}$	forward macroscopic energy transfer rates
W_{Ay-S1}	backward macroscopic energy transfer rates
ψ_y	activator population density change rates
k_{ss}	sensitizer energy migration diffusion constant
∇^2	Laplacian operator
W_{S2-b}	sensitizer surface-related quenching rate

REFERENCES

[1] Auzel, F. Upconversion and anti-stokes processes with f and d ions in solids. *Chemical Society Reviews* **104,** 139-173 (2004).

[2] Bünzli, J.-C. G., Comby, S., Chauvin, A.-S., Vandevyver C. D. B. New opportunities for lanthanide luminescence. *Journal of Rare Earths* **25**, 257-274 (2007).

[3] Deng, R. R., Qin, F., Chen, R. F., Huang, W., Hong, M. H., Liu, X. G. Temporal full-colour tuning through non-steady-state upconversion. *Nature Nanotechnology* **10**: 237-242(2015).

[4] Liu, Y. J., Liu, Y. Q., Yang, X. S., Zheng, X. L., Wen, S. H., Wang, F., Vidal, X., Zhao, J. B., Liu, D. M., Zhou, Z. G., Ma, C. S., Zhou, J. J., James, A. P., Xi, P., Jin, D. Y. Amplified stimulated emission in upconversion nanoparticles for super-resolution nanoscopy. *Nature* **543,** 229-233 (2017).

[5] Tian, G. et al. Mn^{2+} dopant-controlled synthesis of $NaYF_4$: Yb/Er upconversion nanoparticles for in-vivo imaging and drug delivery. *Advanced Materials* **24,** 1226-1231 (2012).

[6] Yang, D. M., Ma, P. A., Hou, Z. Y., Cheng, Z. Y., Li, C. X., Lin, J. Current advances in lanthanide ion (Ln^{3+})-based upconversion nanomaterials for drug delivery. *Chemical Society Reviews* **44**, 1416-1448 (2015).

[7] Kim, W. J.; Nyk, M. and Prasad, P. N. Color coded multilayer photopatterned microstructures using lanthanide (III) ion co-doped $NaYF_4$ nanoparticles with upconversion luminescence for possible applications in security. *Nanotechnology* **20**, 185301 (2009).

[8] Yuan, C. Z., et al. Simultaneous multiple wavelength upconversion in a core-shell nanoparticle for enhanced near infrared light harvesting in a dye-sensitized Solar Cell. *ACS Applied Materials & Interfaces* **6**, 18018-18025 (2014).

[9] Chen, X.; Peng, D. F.; Ju, Q.; Wang, F. Photon upconversion in core-shell nanoparticles. *Chemical Society Reviews* **44**, 1318-1330 (2015).

[10] Chen, G. Y.; Ågren, H.; Ohulchanskyy, T. Y.; Prasad, P. N. Light upconverting core-shell nanostructures: nanophotonic control for emerging applications. *Chemical Society Rev*iews **44**, 1680-1713 (2015).

[11] Marques-Hueso, J., Peretti, R., Abargues, R., Richards, B. S., Seassal, C., Martínez-Pastor, J. P. Photonic crystal-driven spectral concentration for upconversion photovoltaics. *Advanced Optical Materials* **3,** 568-574(2015).

[12] Krieke, G., Sarakovskis, A., Ignatans, R., Gabrusenoks, J. Phase transitions and upconversion luminescence in oxyfluoride glass ceramics containing Ba4Gd3F17 nanocrystals. *Journal of the European Ceramic Society* **37 (4),** 1713-1722 (2017).

[13] Ahmed, E. H. et al. Enhanced UV upconversion emission using plasmonic nanocavities. *Optics Express* 24, 259953 (2016).

[14] Grant, W. J. C. Role of rate equations in the theory of luminescent energy transfer. *Physical Review B* **4,** 648-663 (1971).

[15] Wang, J. et al. Enhancing multiphoton upconversion through energy clustering at sublattice level. *Nature Materials* **13,** 157-163 (2014).

[16] Chen, X. et al. Confining energy migration in upconversion nanoparticles wowards deep ultraviolet lasing. *Nature Communications* **7,** 10304 (2016).

[17] Zuo, J., Sun, D. P., Tu, L. P., Wu, Y. N., Cao, Y. H., Xue, B., Zhang, Y. L., Chang, Y. L., Liu, X. M., Kong, X. G et al. Precisely tailoring upconversion dynamics via energy migration in core-shell nanostructures. *Angewandte Chemie International Edition* **57**, 3054-3058 (2018).

[18] Zuo, J. et al. Revisit of energy transfer upconversion dynamics – the role of energy migration. *Science China: Technological Sciences* **61**, 1301-1308 (2018).

[19] Zhou, B. et al. Probing energy migration through precise control of interfacial energy transfer in nanostructure. *Advanced Materials* **31**, 1806308 (2019).

[20] Liu, J. F.; Fu, T. R. and Shi, C. L. Spatial energy transfer and migration model for upconversion dynamics in core-shell nanostructures. *The Journal of Physical Chemistry C* (2019) 10.1021/acs.jpcc.8b12300.